Chapter 6
Summary and Conclusions

Two fabrication techniques were investigated as they pertain to the assembly of advanced solid oxide fuel cells.

Polymer sphere lithography has been utilized to create two-dimensional metallic networks on fuel cell electrolyte materials. Although the fabrication process involves somewhat imprecise, random elements, the experimental variation from the expected geometries is extremely small. Under fuel cell operating conditions, the structures, and, hence, the 3PB and 2PB area fraction values, exhibit remarkable high temperature stability. These well-defined and well-behaved electrode structures access a wide range of 3PB regimes, lending themselves to future mechanistic studies on electrolyte-electrode material systems, as well as providing a strong experimentally correlated basis for computational modeling. Beyond mechanistic studies, these anti-dot structures have served as platforms for fabrication of three-dimensional electrodes.

The cathodic electrochemical deposition of undoped and Sm-doped ceria has been developed in templated and template-free configurations to produce a variety of tunable anode microstructures. The strictly chemical nature of the deposition step allows these electronically insulating coatings to deposit onto non-conducting areas of substrates, insofar as they are close enough to an exposed metal surface. The end result is ubiquitous CeO_2 coatings on thin, porous metallic networks overlaid onto YSZ/porous metal substrates, with quality metal|CeO_2 and YSZ|CeO_2 interfaces, which are morphologically

stable at high temperatures and reducing atmospheres. Deposition was also definitively shown to occur on two MIEC, fuel cell cathode materials—BSCF and SCN.

To probe the activity of CELD Sm-doped ceria anodes, detailed, morphologically-driven ACIS analyses were conducted, revealing two co-dominant, resistive processes for metal network embedded configurations. The LF arc was determined to be surface-related; the HF arc was determined to be configurationally related, in particular to the resistance of electron migration through the SDC deposit on top of the metal regions, and the resulting restriction of the field lines to the nominal 3PB region. The LF arc was therefore taken to represent the true measure of surface activity for CELD ceria. The lowest extrapolated ASR values for this arc were shown to be in the range of 1.3 – 6.8 $m\Omega\ cm^2$ at 650 °C in 97% H_2 and 3% H_2O.

Appendix A
ImageJ Analysis Details

The following describes the analytical approach to identifying and characterizing the pores of the anti-dot networks using the ImageJ software described in Chapter 2. The process is briefly illustrated in Fig. A.1. First, an as-taken grayscale SEM image is imported into ImageJ (Fig. A.1a); then, the data bar region is cropped and the rest of the image is converted into a true black-and-white image (Fig. A.1b). The ImageJ user can define a grayscale threshold cutoff value, above which the associated pixels are converted to purely black, and below which the pixels are converted to purely white. Consequently, the ideal SEM image to be analyzed is one where there is significant grayscale contrast between the circular pores exposing the electrolyte surface, and the metal network lying on top. Secondary electron imaging mode was chosen owing to its inherent contrast associated with topographical features (recall that the metal network is 200-400 nm thick). Back-scattered mode, which provides elemental materials contrast, added anywhere from 5-15% areal error due to pore shading; and in-lens mode, known for its high contrast imaging ability, was found to provide inconsistencies related to charging effects from the non-conducting YSZ. Care was taken to provide qualitatively consistent contrast in the SEM images across the entirety of the substrate, to ensure accurate and uniform threshold application.

The resulting image (Fig.A.1b) is now a mixture of connected and disconnected black objects, which ImageJ can identify automatically. Problems arise, however, due to dark pixels that are not pore-related. The smaller dark objects can be automatically removed, and the image consequently cleaned up, as in Fig. A.1c. However, the messy,

larger unwanted dark objects remain—these are originally void areas left uncovered during the PS deposition process and result in planar metal regions after the thermal evaporation step. Fortunately, these areas are never circular, so a “circularity” filter can be applied when identifying objects. This filter is applied between Fig. A.1c and d. ImageJ defines a circularity of 1 to be a perfect circle, and 0 to be a straight line. In this way, fractal objects like these metal regions can be removed from the counting. Fig. A.1d is the final pictorial output of the ImageJ process, and shows which objects have been identified. Pore area (2PB), perimeter (3PB), and total pore coverage are all automatically enumerated. Depending on the pore size to be evaluated, different magnification was necessary to ensure accuracy—it was found that no more than 1500 pores could be evaluated from one image and retain acceptable levels of accuracy.

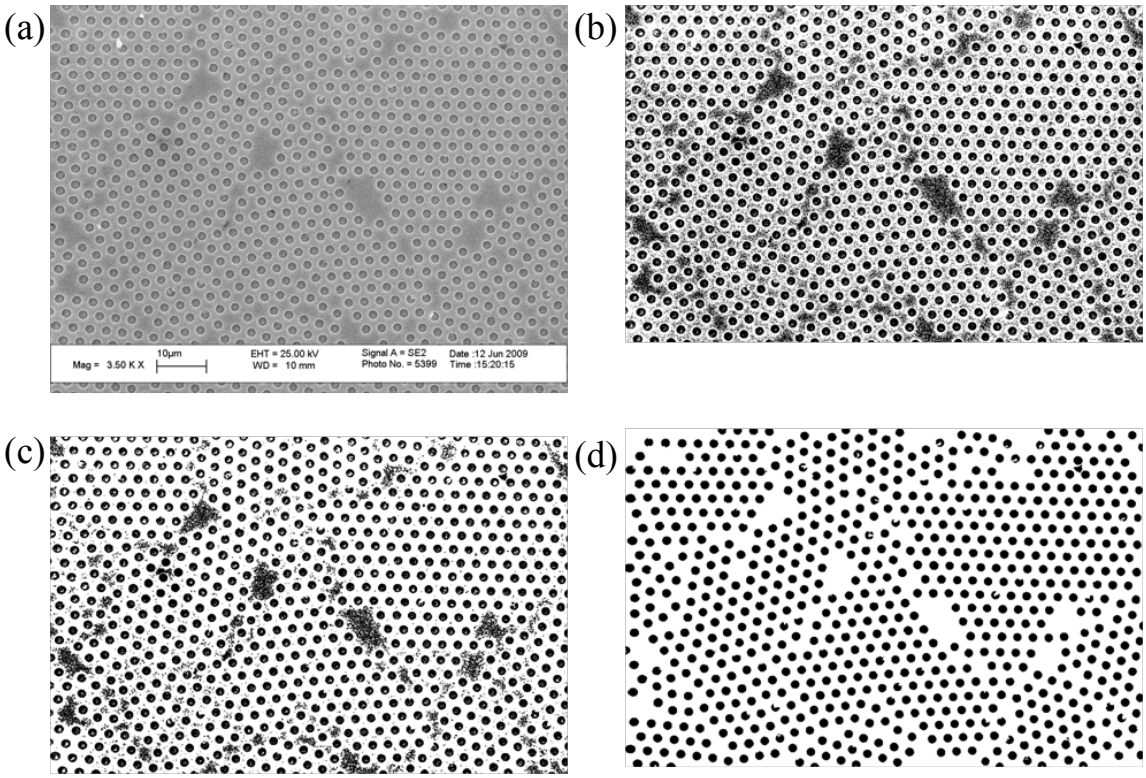

Fig A.1. The ImageJ image analysis process: (a) an as-taken SEM image; (b) cropping and conversion to black-and-white; (c) image clean-up; and (d) final image identifying the pores.

Appendix B
Additional Images

B.1 Additional CELD Images

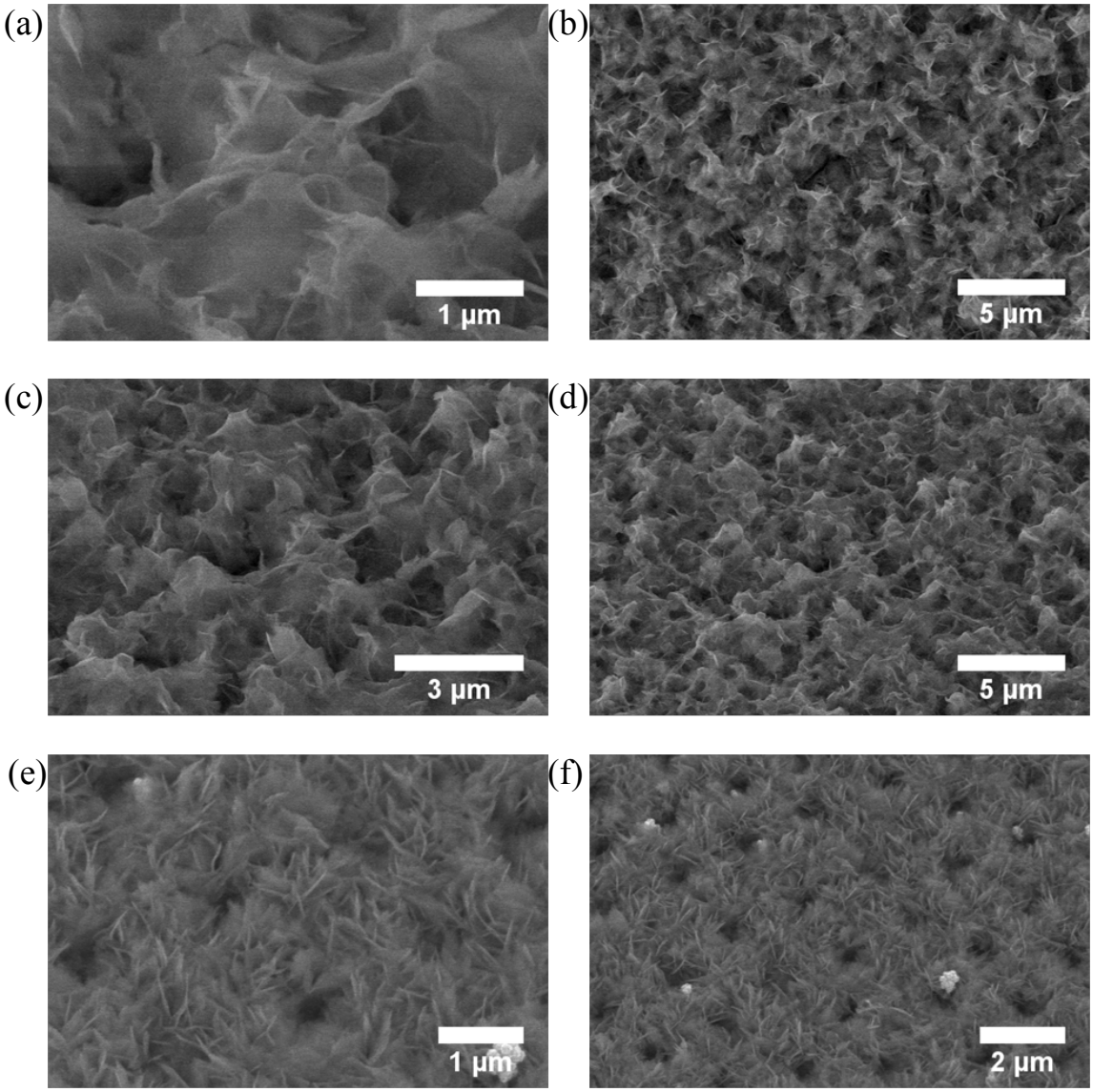

Fig. B.1. Angled (45°) SEM images of the HSA microstructure deposited at 0.8 mA cm^{-2} with a 0.05 M doped electrolyte for 5 minutes (a through d); and a 0.1 M undoped electrolyte for 5 minutes (e and f).

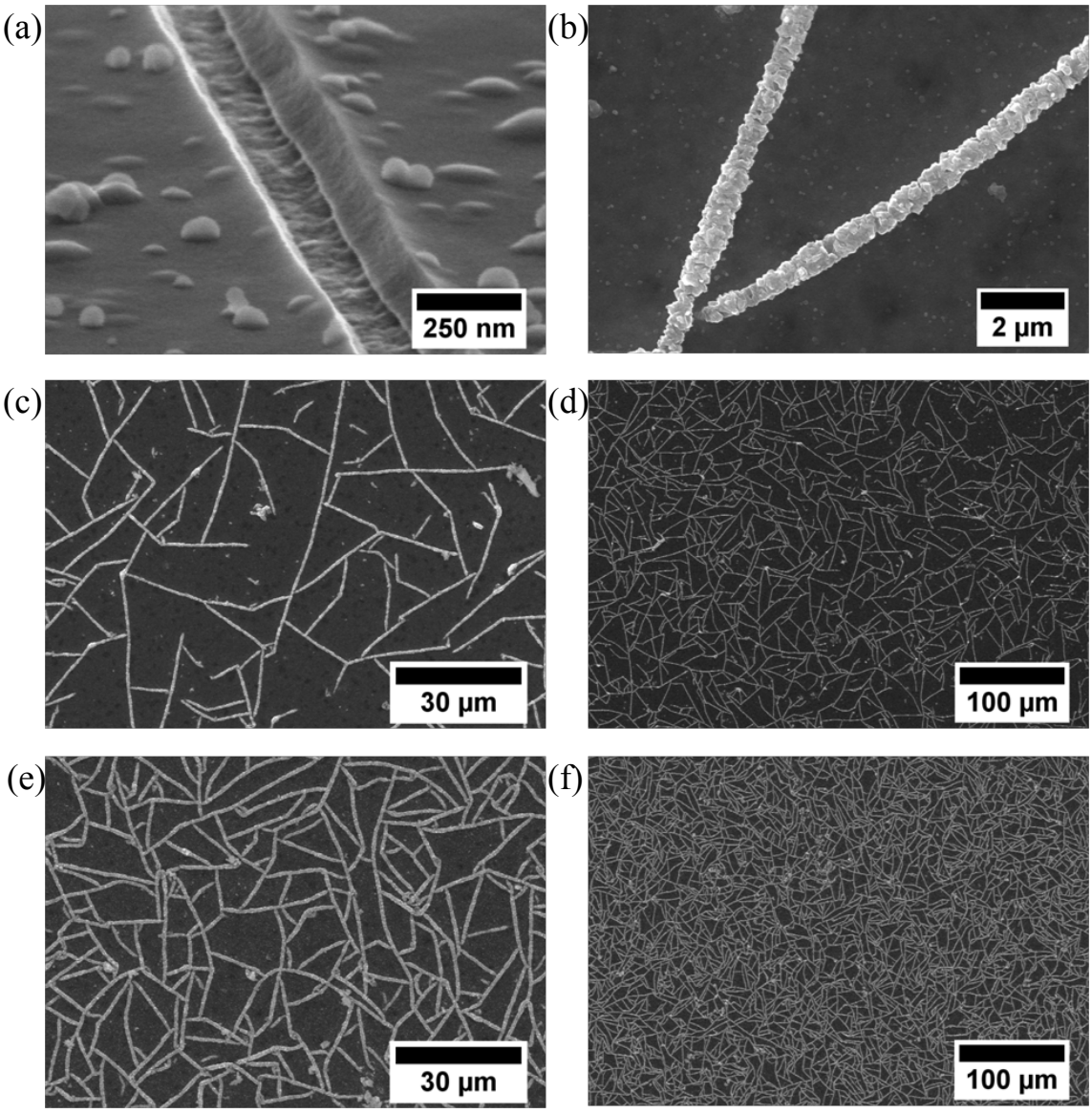

Fig. B.2. SEM images of CELD thin films of ceria deposited at -0.55 V vs. SCE with the doped + H_2O_2 electrolyte on thin films of Ni on silicon substrates for different times: (a) – (d) 5 minutes; (e) and (f) 10 minutes. (a) shows an as-deposited crack that forms for thicknesses greater than 300 nm ceria films. (b) – (f) are images taken after annealing in an Ar atmosphere at 600 °C for 10 hours. The white strips are crack areas that originally formed as-deposited as in (a), but the exposed Ni metal has oxidized to NiO and volume-expanded out of the crack. The higher degree of cracking for the thicker film in (e) and (f) is easily visualized.

The following TEM images are taken from the same sample shown in Fig. 3.24. (a) is a bright-field image, and (b) through (d) are corresponding dark-field images taken at different tilting angles to highlight various grain orientations, which consequently appear white. (e) is the selected-area diffraction pattern, labeled with approximate lattice parameters. (f) is a HRTEM view of the polycrystalline deposit.

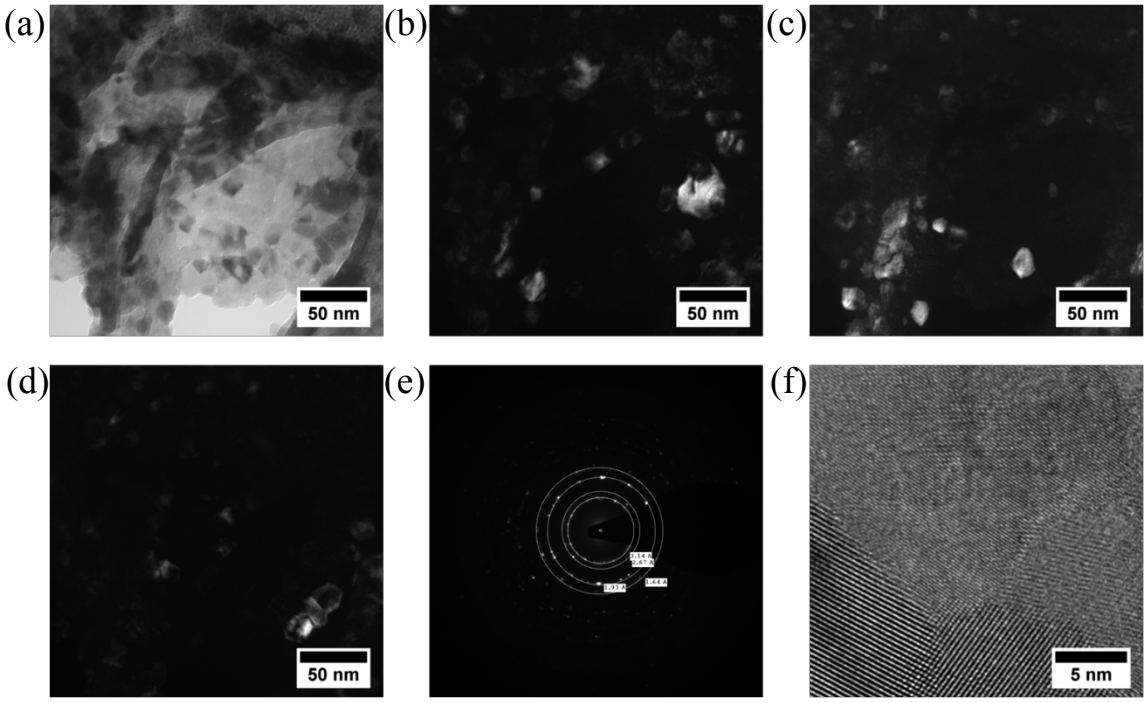

Fig. B.3. TEM images taken from the same sample as in Fig. 3.24. See description above.

B.2 Additional AAO Images

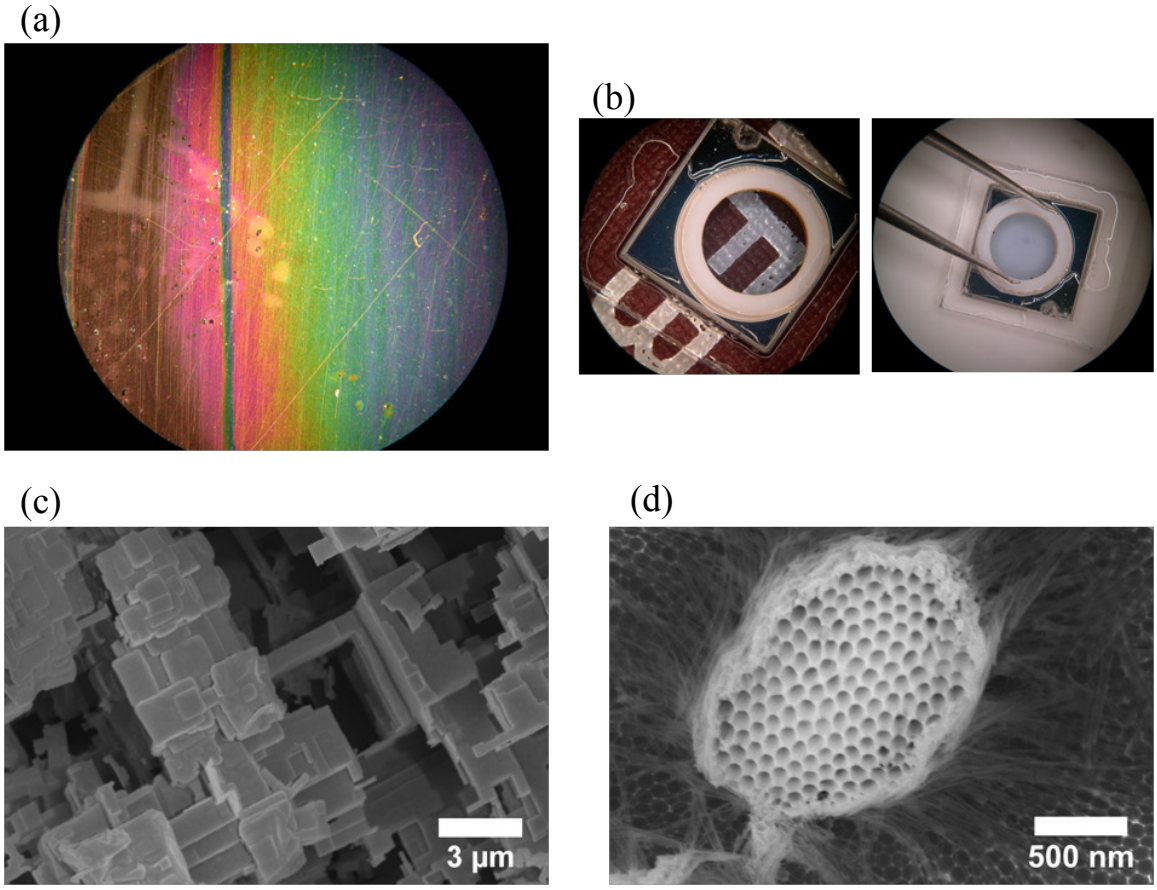

Fig. B.4. Various AAO images: (a) optical image of thin film interference patterns resulting from the complete anodic oxidation of sputtered Al on a glass slide; (b) when the sputtered Al is sectioned off, complete anodic oxidation results in a transparent window, seen here on a YSZ single crystal substrate 1 x 1 cm; (c) if Al metal is left in the oxalic acid electrolyte too long, crystallographic etching occurs; and (d) when the AAO template is etched in chromic and phosphoric acid, incomplete template removal results in peculiar structures.

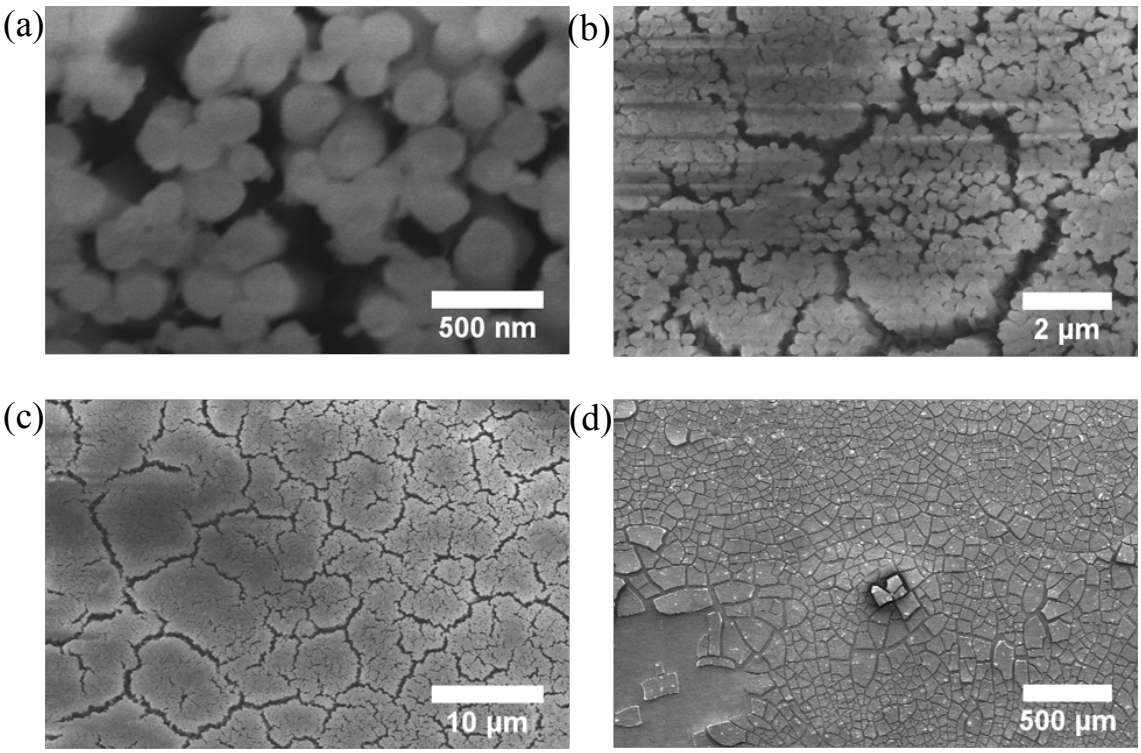

Fig. B.5. CELD ceria nanowires from the same sample shown in Fig. 5.7. (a) – (c) are after etching in 3 M NaOH for 2.5 minutes. (d) is as-deposited, showing the scale-like overgrowth of ceria once deposition was complete in the entire pore lengths of the AAO template.

B.3 Additional Inverse Opal Images

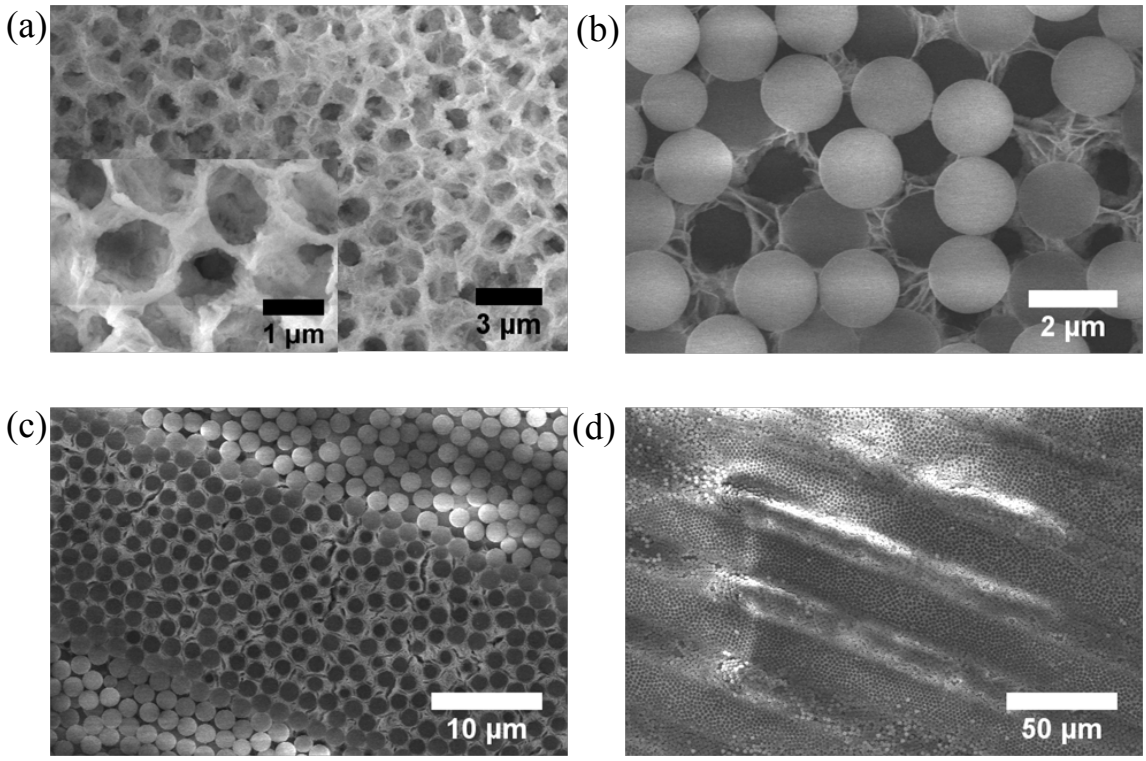

Fig. B.6. Various SEM images of inverse opal structures from the same samples as in Fig. 5.9.

B.4 Additional MIEC Substrate Images

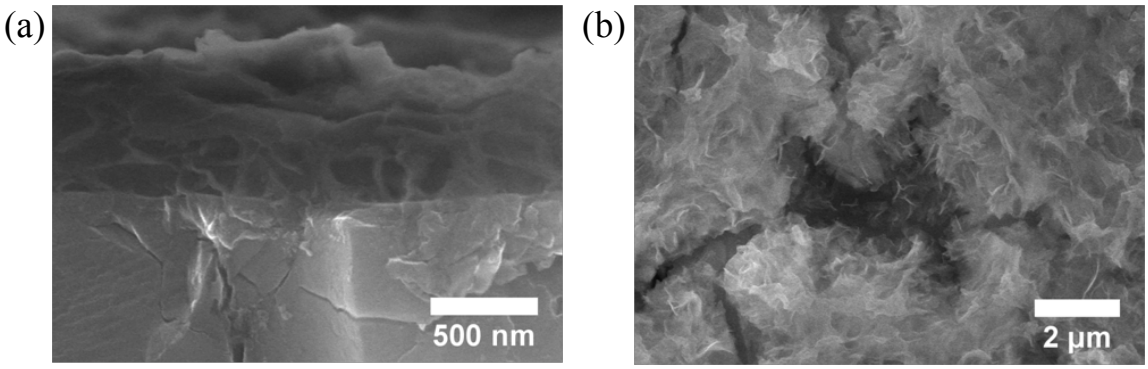

Fig. B.7. SEM images of HSA ceria grown on BSCF at 0.8 mA cm^{-2} for: (a) 1 minute, showing a good interface between ceria and BSCF; and (b) 5 minutes, showing HSA bridging of a pore in the underlying BSCF filled with nail polish (dark area).

B.5 Additional Oxidation Protection Coating Images

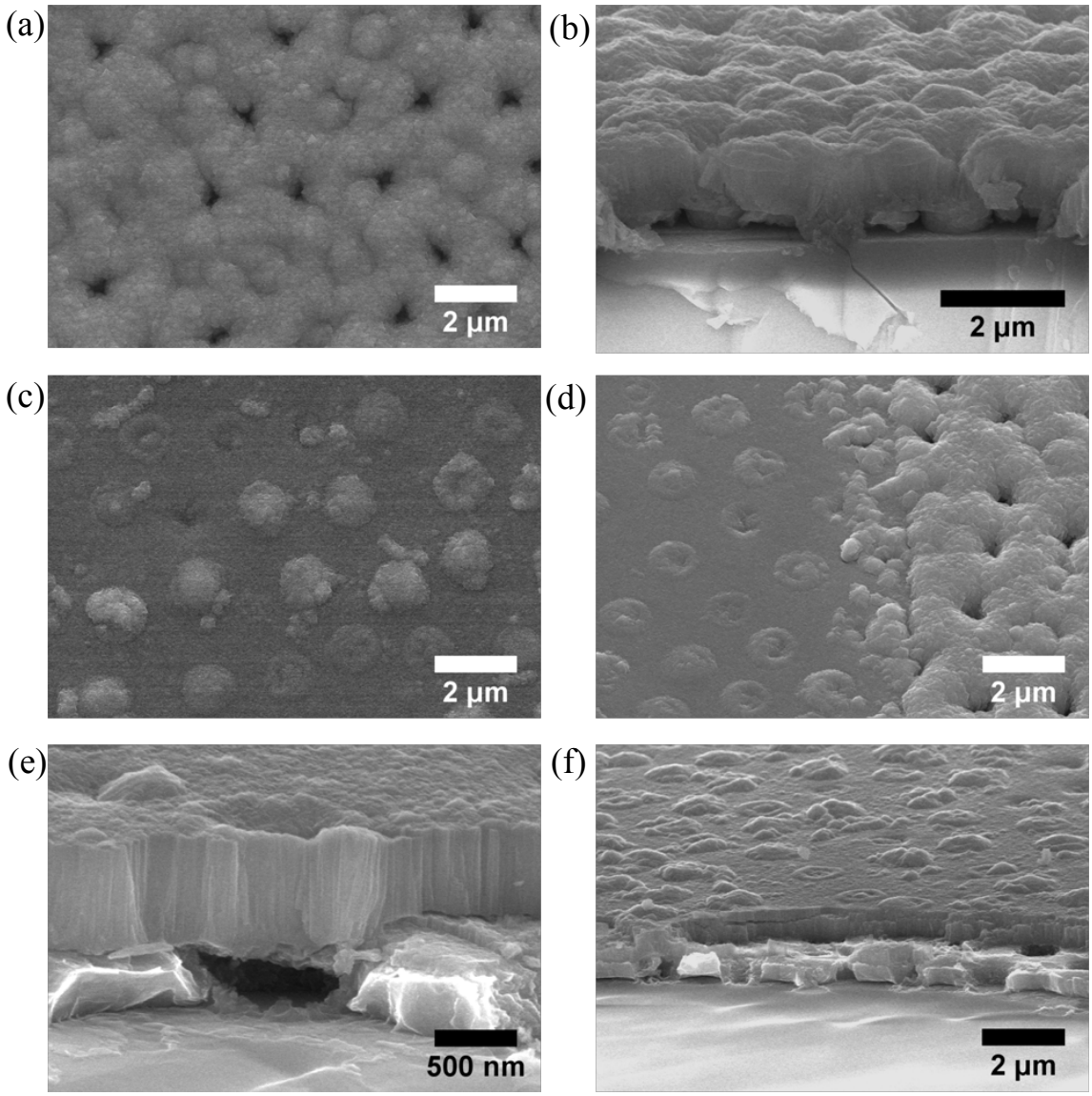

Fig. B.8. SEM images of the oxidative protection coating action of CELD ceria, as in Fig. 5.11: (a) and (b) are the Ni anti-dot areas uncovered by CELD; (c) is the area covered by CELD; (d) is the border between the covered and uncovered CELD regions; (e) and (f) are cross-sectional views of the CELD covered regions. All images have a PLD top coating.

Appendix C
Alternate SOFC Microstructure Fabrication Routes

C.1 Solution Impregnation into AAO Templates

A straightforward solution-phase approach to filling the pores of AAO templates was reported in [124]. Briefly, an AAO template is immersed into a 2.5 M cerium nitrate bath for 4 hours, dried at 50 °C for 4 hours, and then thermally treated from 150 – 500 °C to solidify the nanowires/tubes. In an attempt to mimic this approach, an identical cerium nitrate solution was employed with unaided impregnation (Fig. C.1), sonication-assisted impregnation (Fig. C.2), stirring-assisted impregnation (Fig. C.3), and a combination of stirring- and sonication-assisted impregnation (Fig. C.4). The last approach worked best, in terms of filling fraction of the AAO pores. However, any solution-phase route to making nanowires suffers from a common drawback—there is no inherent attachment to an underlying substrate. Attempts were made to thermally sinter nanowires made from these methods to a YSZ underlying substrate while they were still held in place by the surrounding AAO matrix, but thermal treatment of the assembly has the undesirable side-effect of crystallizing the alumina into an un-etchable form. Prolonged treatment in acids, e.g., chromic and phosphoric, and bases, e.g. NaOH, had zero effect, as can be seen in Fig. C.5. Accordingly, this method was abandoned.

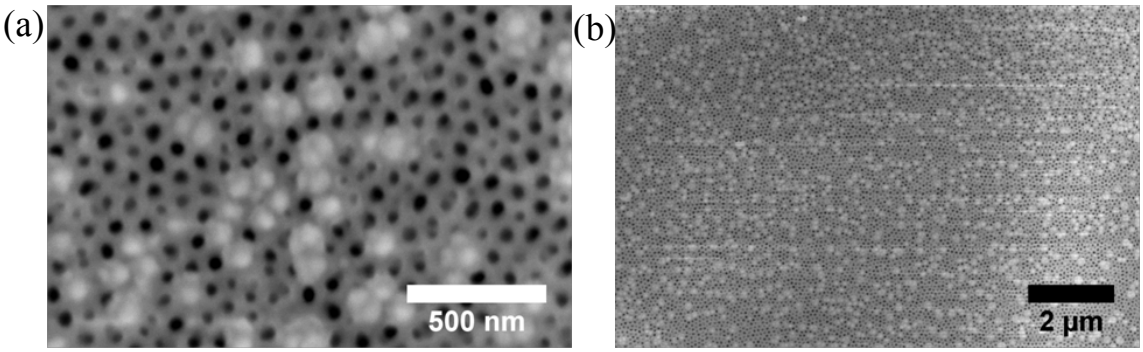

Fig. C.1. Ceria nanowires partially filling the pore of an AAO template after unaided solution phase impregnation.

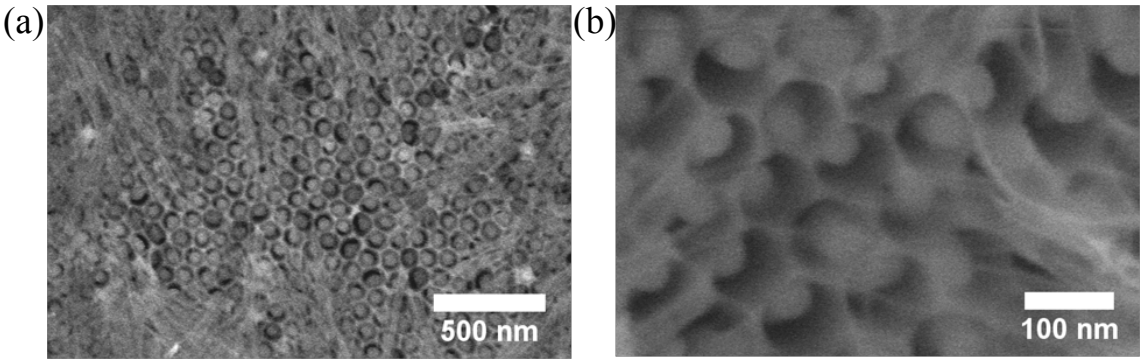

Fig. C.2. Ceria nanowires partially filling the pore of an AAO template after sonicated solution phase impregnation.

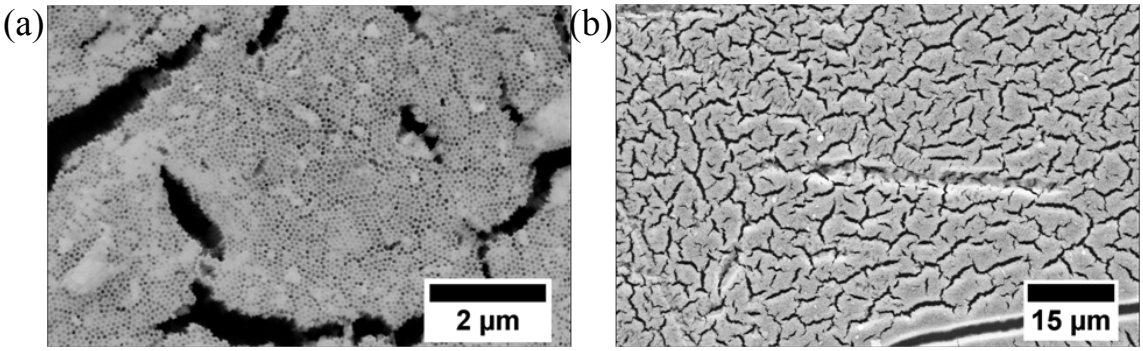

Fig. C.3. Ceria nanowires partially filling the pore of an AAO template after stirred solution phase impregnation.

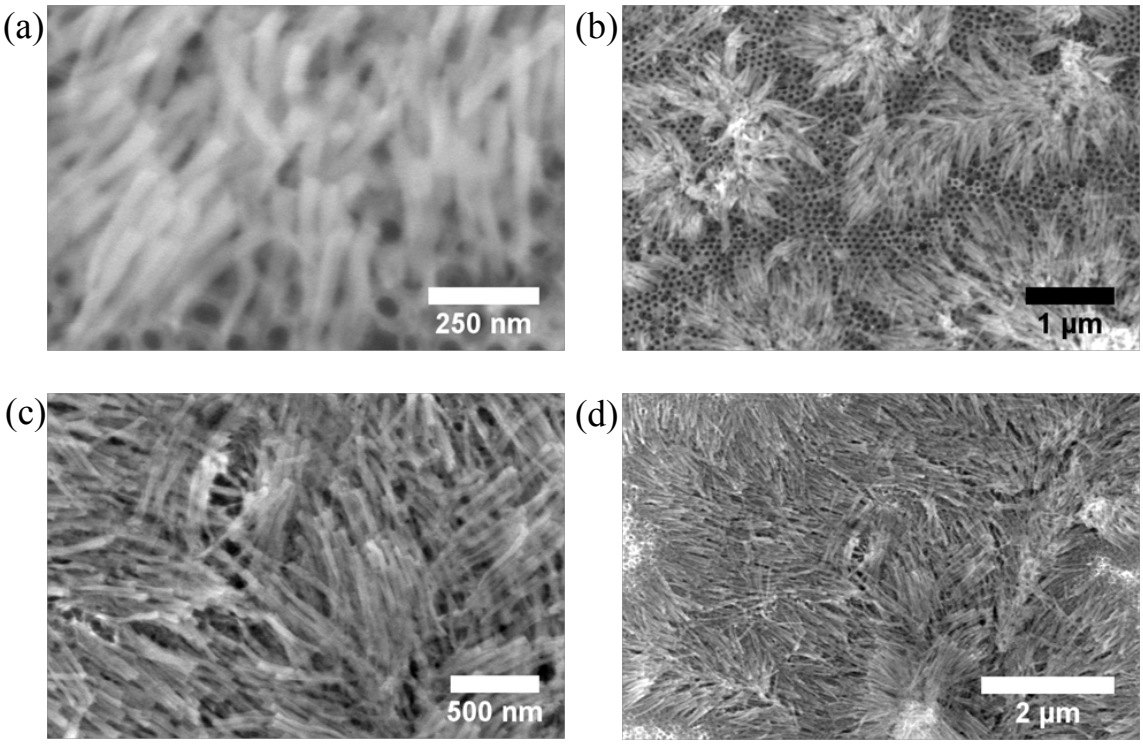

Fig. C.4. Ceria nanowires partially filling the pore of an AAO template after sonicated/stirred solution phase impregnation.

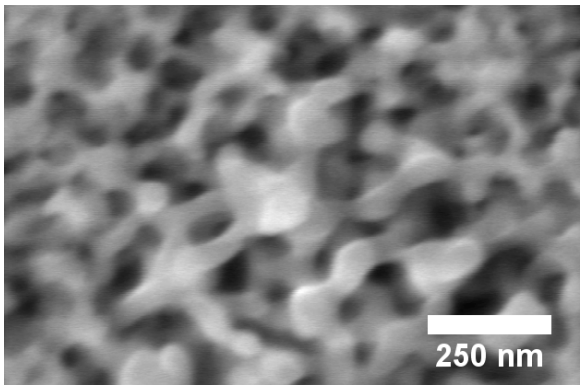

Fig. C.5. SEM image of an AAO template after thermal treatment at 1100°C for 5 hours in air, and after unsuccessful, repeated attempts to etch the template in chromic/phosphoric acid mixtures and NaOH.

C.2 Copper Nanowire Synthesis

It has been known since the 1960's that copper oxide nanowires form spontaneously on the outer surface of the oxide scale during thermal treatment of copper metal at temperatures exceeding 400 °C [125-129]. The aspect ratio and number density can be altered by changing the growth temperature and surrounding atmosphere. This approach works well with bulk copper foil substrates, and also works on copper thin films grown on a supporting substrate. However, the copper metal thin films must be greater than 500 nm in order to produce an appreciable amount of CuO nanowires. The as-produced CuO nanowires can be subsequently reduced in a hydrogen plasma to copper metal [130]. Higher power density plasmas can significantly alter the original CuO morphology, but lower power density plasmas can completely reduce the CuO to Cu without much morphological evolution. Below are selected images from this approach. The combination of copper metal thin film thickness limitations and the inconsistencies of the process lead to its abandonment.

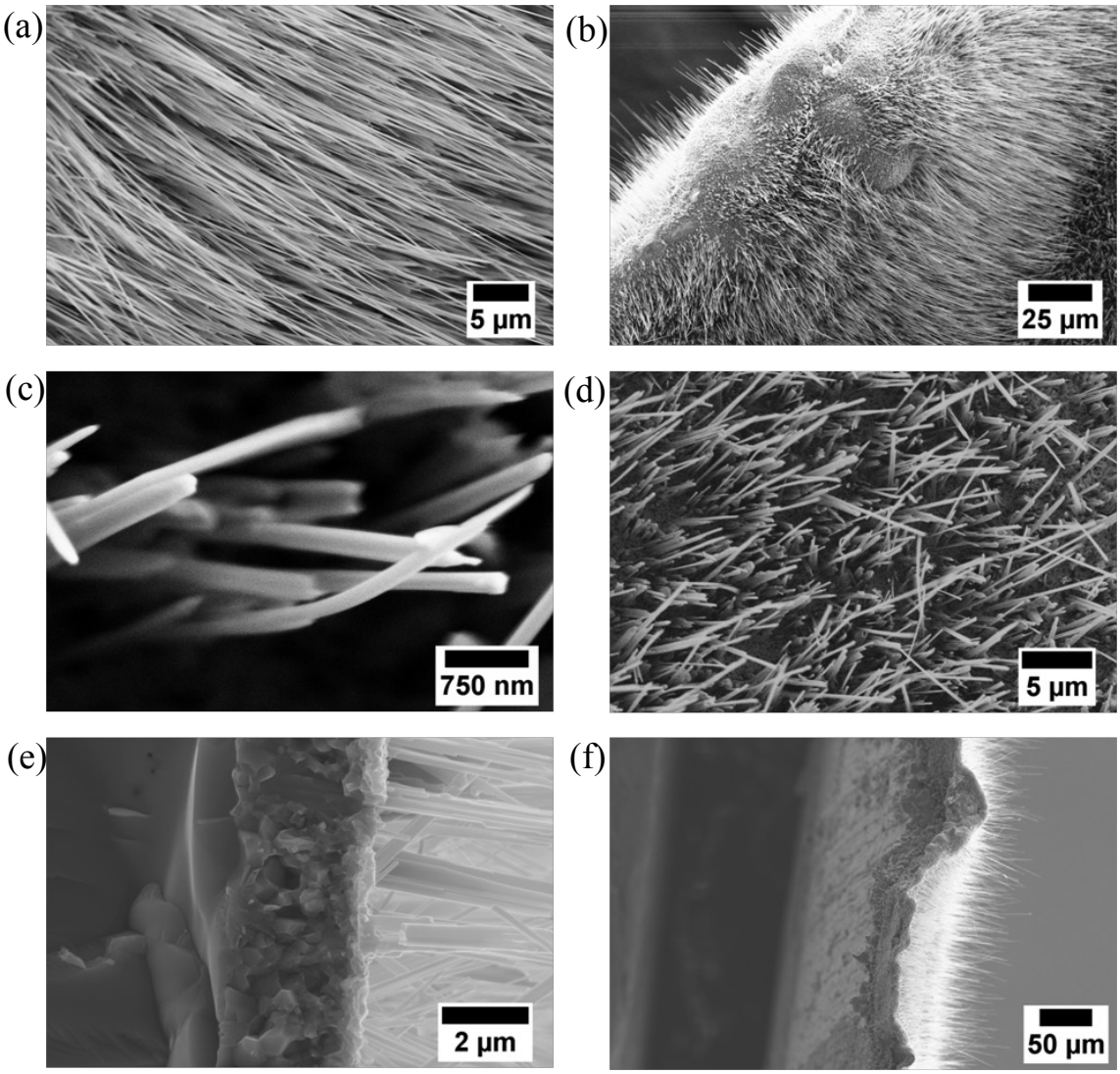

Fig. C.6. SEM images of CuO nanowires grown at ~500 °C for a couple of hours in ambient air from a 0.25 mm Cu foil.

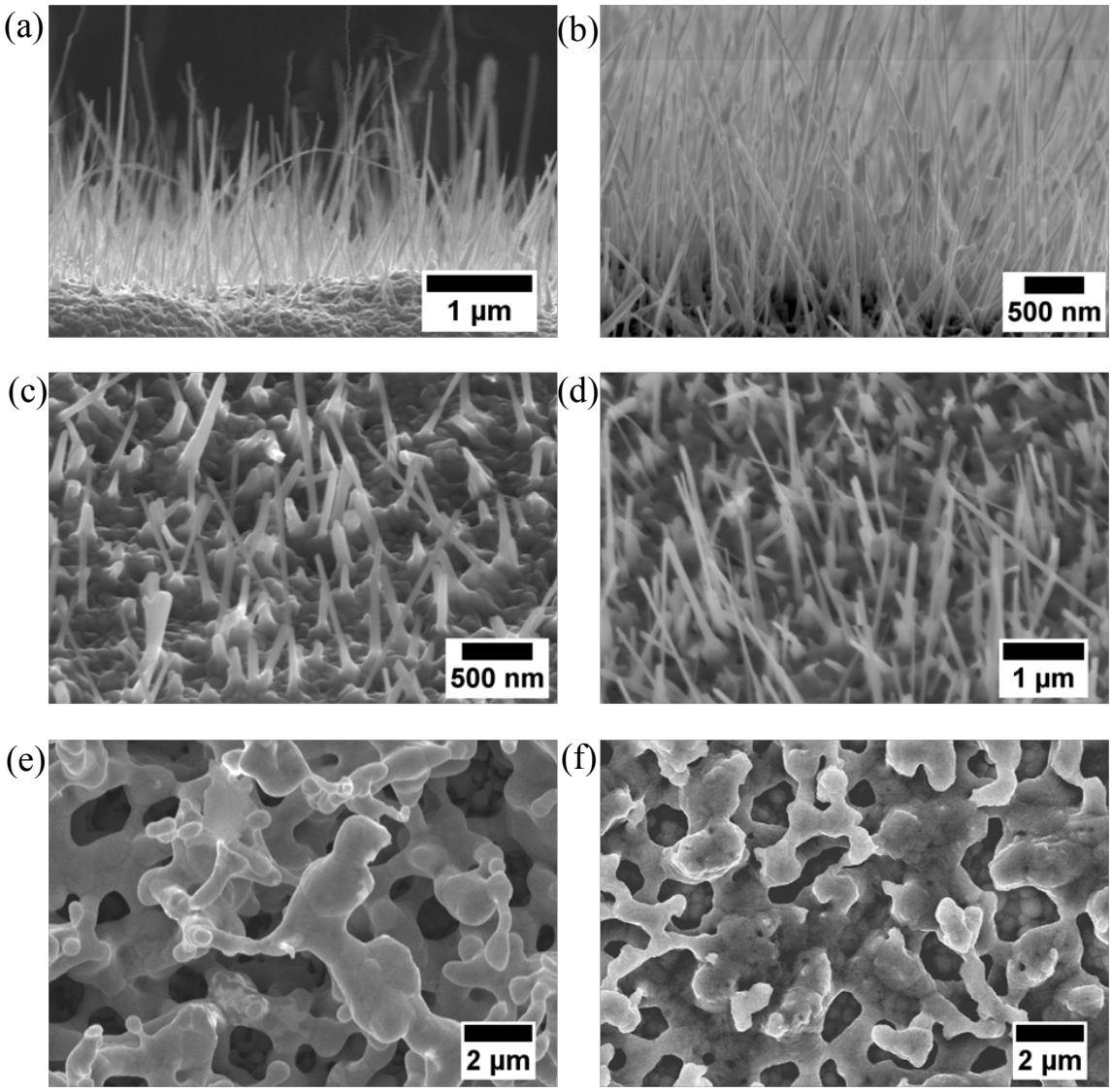

Fig. C.7. SEM images of CuO nanowires grown at ~500 °C for a couple of hours in ambient air from a thin film of Cu thermally evaporated onto polycrystalline SDC pellets (a) – (d); (e) and (f) show the highly evolved morphology of CuO nanowires to a porous Cu film after they have been reduced in a high power density hydrogen plasma for ~5 minutes.

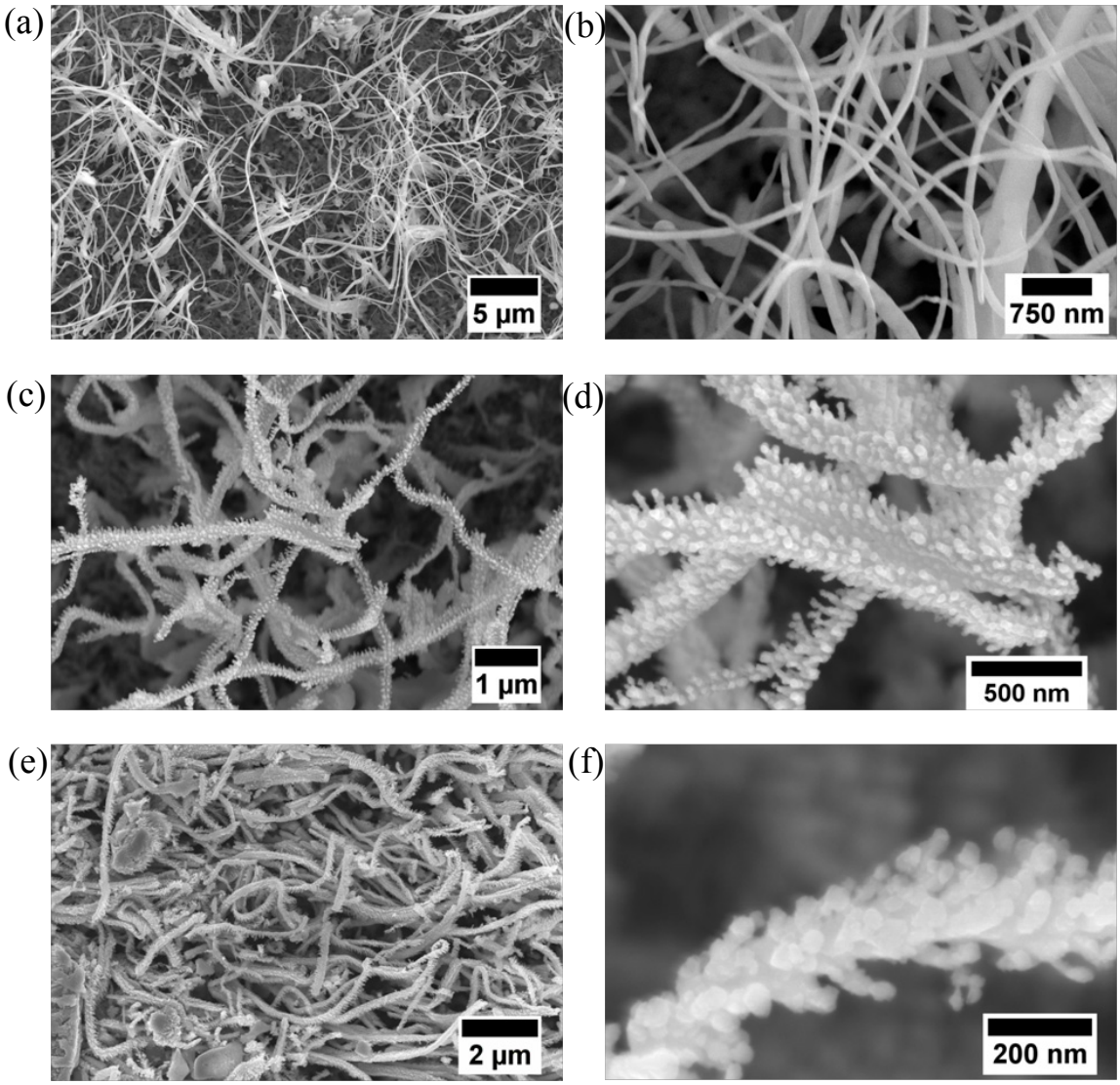

Fig. C.8. SEM images of Cu nanowire structures resulting from a moderate power density hydrogen plasma reduction of the CuO nanowires picture in Fig. C.6. (a) and (b) are treated with the plasma for a couple of minutes; (c) – (f) have been treated for greater than 5 minutes, and show some texturing on the nanoscale as a result.

References

1. Chueh, W.C., *Electrochemical & Thermochemical Behavior of CeO2-δ*, in *Materials Science*. 2011, California Institute of Technology.
2. Tarascon, J.M. and M. Armand, *Issues and challenges facing rechargeable lithium batteries.* Nature, 2001. **414**(6861): p. 359-367.
3. Zhao, X., et al., *The role of nanomaterials in redox-based supercapacitors for next generation energy storage devices.* Nanoscale, 2011. **3**(3): p. 839-855.
4. Zhang, H., G.P. Cao, and Y.S. Yang, *Carbon nanotube arrays and their composites for electrochemical capacitors and lithium-ion batteries.* Energy & Environmental Science, 2009. **2**(9): p. 932-943.
5. Carrette, L., K.A. Friedrich, and U. Stimming, *Fuel cells: Principles, types, fuels, and applications.* Chemphyschem, 2000. **1**(4): p. 162-193.
6. Ryan O'Hayre, S.-W.C., Whitney Colella, Fritz B. Prinz, *Fuel Cell Fundamentals*. 2006: John Wiley & Sons.
7. Hulteen, J.C. and R.P. Vanduyne, *Nanosphere Lithography - a Materials General Fabrication Process for Periodic Particle Array Surfaces.* Journal of Vacuum Science & Technology a-Vacuum Surfaces and Films, 1995. **13**(3): p. 1553-1558.
8. Haynes, C.L. and R.P. Van Duyne, *Nanosphere lithography: A versatile nanofabrication tool for studies of size-dependent nanoparticle optics.* Journal of Physical Chemistry B, 2001. **105**(24): p. 5599-5611.
9. Ho, K.C. and J. Jorne, *Electrochemical Impregnation of Nickel-Hydroxide - Flow-through Vs Stagnant Electrodes.* Journal of the Electrochemical Society, 1990. **137**(1): p. 149-158.
10. Indira, L. and P.V. Kamath, *Electrogeneration of Base by Cathodic Reduction of Anions - Novel One-Step Route to Unary and Layered Double Hydroxides (Ldhs).* Journal of Materials Chemistry, 1994. **4**(9): p. 1487-1490.
11. Yamazaki, Y., R. Hernandez-Sanchez, and S.M. Haile, *High Total Proton Conductivity in Large-Grained Yttrium-Doped Barium Zirconate.* Chemistry of Materials, 2009. **21**(13): p. 2755-2762.

12. Magraso, A., et al., *Development of Proton Conducting SOFCs Based on LaNbO4 Electrolyte - Status in Norway.* Fuel Cells, 2011. **11**(1): p. 17-25.
13. Tucker, M.C., *Progress in metal-supported solid oxide fuel cells: A review.* Journal of Power Sources, 2010. **195**(15): p. 4570-4582.
14. Haile, S.M., *Fuel cell materials and components.* Acta Materialia, 2003. **51**(19): p. 5981-6000.
15. Eguchi, K., et al., *ELECTRICAL-PROPERTIES OF CERIA-BASED OXIDES AND THEIR APPLICATION TO SOLID OXIDE FUEL-CELLS.* Solid State Ionics, 1992. **52**(1-3): p. 165-172.
16. Tsai, T.P. and S.A. Barnett, *Effect of mixed-conducting interfacial layers on solid oxide fuel cell anode performance.* Journal of the Electrochemical Society, 1998. **145**(5): p. 1696-1701.
17. Steele, B.C.H., *Appraisal of Ce1-yGdyO2-y/2 electrolytes for IT-SOFC operation at 500 degrees C.* Solid State Ionics, 2000. **129**(1-4): p. 95-110.
18. Fleig, J., *Solid oxide fuel cell cathodes: Polarization mechanisms and modeling of the electrochemical performance.* Annual Review of Materials Research, 2003. **33**: p. 361-382.
19. Shao, Z.P. and S.M. Haile, *A high-performance cathode for the next generation of solid-oxide fuel cells.* Nature, 2004. **431**(7005): p. 170-173.
20. Yu, H.C., et al., *Electrochemical characterization and performance evaluation of intermediate temperature solid oxide fuel cell with La0.75Sr0.25CUO2.5-delta cathode.* Journal of Power Sources, 2005. **152**(1): p. 22-26.
21. Pena-Martinez, J., et al., *Performance of XSCoF (X = Ba, La and Sm) and LSCrX ' (X ' = Mn, Fe and Al) perovskite-structure materials on LSGM electrolyte for IT-SOFC.* Electrochimica Acta, 2007. **52**(9): p. 2950-2958.
22. Zhang, P., et al., *Sr2CoMoO6 anode for solid oxide fuel cell running on H-2 and CH4 fuels.* Journal of Power Sources, 2011. **196**(4): p. 1738-1743.
23. Tao, S.W. and J.T.S. Irvine, *Synthesis and characterization of (La0.75Sr0.25)Cr0.5Mn0.5O3-delta, a redox-stable, efficient perovskite anode for SOFCs.* Journal of the Electrochemical Society, 2004. **151**(2): p. A252-A259.

24. Atkinson, A., et al., *Advanced anodes for high-temperature fuel cells.* Nature Materials, 2004. **3**(1): p. 17-27.

25. Jiang, S.P. and S.H. Chan, *A review of anode materials development in solid oxide fuel cells.* Journal of Materials Science, 2004. **39**(14): p. 4405-4439.

26. Ciucci, F., et al., *Surface reaction and transport in mixed conductors with electrochemically-active surfaces: a 2-D numerical study of ceria.* Physical Chemistry Chemical Physics, 2011. **13**(6): p. 2121-2135.

27. Chueh, W.C., W. Lai, and S.M. Haile, *Electrochemical behavior of ceria with selected metal electrodes.* Solid State Ionics, 2008. **179**(21-26): p. 1036-1041.

28. Gross, M.D., J.M. Vohs, and R.J. Gorte, *A strategy for achieving high performance with SOFC ceramic anodes.* Electrochemical and Solid State Letters, 2007. **10**(4): p. B65-B69.

29. Lu, C., et al., *A comparison of Cu-ceria-SDC and Au-ceria-SDC composites for SOFC anodes*, in *Solid Oxide Fuel Cells Viii*, S.C. Singhal and M. Dokiya, Editors. 2003, Electrochemical Society Inc: Pennington. p. 773-780.

30. Marina, O.A., et al., *A solid oxide fuel cell with a gadolinia-doped ceria anode: preparation and performance.* Solid State Ionics, 1999. **123**(1-4): p. 199-208.

31. W.C. Chueh, Y.H., S.M. Haile, *High Electrochemical Activity of the Oxide Phase in Model Ceria-Pt and Ceria-Ni Composite Anode.* Submitted 2011.

32. Chueh, W.C. and S.M. Haile, *Electrochemical studies of capacitance in cerium oxide thin films and its relationship to anionic and electronic defect densities.* Physical Chemistry Chemical Physics, 2009. **11**(37): p. 8144-8148.

33. Wilson, J.R., et al., *Three-dimensional reconstruction of a solid-oxide fuel-cell anode.* Nature Materials, 2006. **5**(7): p. 541-544.

34. Mizusaki, J., et al., *Preparation of Nickel Pattern Electrodes on Ysz and Their Electrochemical Properties in H2-H2o Atmospheres.* Journal of the Electrochemical Society, 1994. **141**(8): p. 2129-2134.

35. Bieberle, A., L.P. Meier, and L.J. Gauckler, *The electrochemistry of Ni pattern anodes used as solid oxide fuel cell model electrodes.* Journal of the Electrochemical Society, 2001. **148**(6): p. A646-A656.

36. Baumann, F.S., et al., *Quantitative comparison of mixed conducting SOFC cathode materials by means of thin film model electrodes.* Journal of the Electrochemical Society, 2007. **154**(9): p. B931-B941.

37. Bieberle, A. and L.J. Gauckler, *State-space modeling of the anodic SOFC system Ni, H-2-H2O vertical bar YSZ.* Solid State Ionics, 2002. **146**(1-2): p. 23-41.

38. Goodwin, D.G., et al., *Modeling Electrochemical Oxidation of Hydrogen on Ni-YSZ Pattern Anodes.* Journal of the Electrochemical Society, 2009. **156**(9): p. B1004-B1021.

39. Piao, J.H., et al., *A study of process parameters of LSM and LSM-YSZ composite cathode films prepared by screen-printing.* Journal of Power Sources, 2008. **175**(1): p. 288-295.

40. Beckel, D., et al., *Thin films for micro solid oxide fuel cells.* Journal of Power Sources, 2007. **173**(1): p. 325-345.

41. De Jonghe, L.C., C.P. Jacobson, and S.J. Visco, *Supported electrolyte thin film synthesis of solid oxide fuel cells.* Annual Review of Materials Research, 2003. **33**: p. 169-182.

42. Therese, G.H.A. and P.V. Kamath, *Electrochemical synthesis of metal oxides and hydroxides.* Chemistry of Materials, 2000. **12**(5): p. 1195-1204.

43. Zhitomirsky, I., *Cathodic electrodeposition of ceramic and organoceramic materials. Fundamental aspects.* Advances in Colloid and Interface Science, 2002. **97**(1-3): p. 279-317.

44. Bhattacharya, R., et al., *Electrodeposited biaxially textured buffer layer for YBa2Cu3O7-delta (YBCO) superconductor oxide films.* Journal of the Electrochemical Society, 2006. **153**(5): p. C273-C276.

45. Zhitomirsky, I. and A. Petric, *Electrochemical deposition of ceria and doped ceria films.* Ceramics International, 2001. **27**(2): p. 149-155.

46. Kamada, K., N. Enomoto, and J. Hojo, *Optimization of electrochemical synthesis conditions for dense and doped ceria thin films.* Electrochimica Acta, 2009. **54**(27): p. 6996-7000.

47. Bocchetta, P., M. Santamaria, and F. Di Quarto, *Electrosynthesis of Ce-Co mixed oxide nanotubes with high aspect ratio and tunable composition.* Electrochemical and Solid State Letters, 2008. **11**(3): p. K27-K30.

48. Zhitomirsky, I. and A. Petric, *Electrolytic and electrophoretic deposition of CeO2 films.* Materials Letters, 1999. **40**(6): p. 263-268.

49. Zhang, C.J., et al., *Heterogeneous films of ordered CeO2/Ni concentric nanostructures for fuel cell applications.* Physical Chemistry Chemical Physics, 2010. **12**(17): p. 4295-4300.

50. Zivkovic, L., et al., *Effect of samarium addition and annealing on the properties of electrodeposited ceria thin films.* Thin Solid Films, 2011. **519**(11): p. 3538-3543.

51. Lair, V., et al., *Synthesis and characterization of cerium oxide by electrochemical methods.* Physica Status Solidi C - Current Topics in Solid State Physics, Vol 5, No 11 2008, 2008. **5**(11): p. 3492-3495

135.

52. Elbelghiti, H., et al., *Electrodeposition of Ceria on Stainless Steel for SOFC Interconnect Applications.* Solid Oxide Fuel Cells 10 (Sofc-X), Pts 1 and 2, 2007. **7**(1): p. 2391-2397

2646.

53. Hamlaoui, Y., et al., *Cathodic electrodeposition of cerium-based oxides on carbon steel from concentrated cerium nitrate solutions Part I. Electrochemical and analytical characterisation.* Materials Chemistry and Physics, 2009. **113**(2-3): p. 650-657.

54. Kulp, E.A., et al., *Electrodeposition of nanometer-thick ceria films by oxidation of cerium(III)-acetate.* Solid State Ionics, 2007. **178**(11-12): p. 749-757.

55. Li, F.B., R.C. Newman, and G.E. Thompson, *In situ atomic force microscopy studies of electrodeposition mechanism of cerium oxide films: Nucleation and growth out of a gel mass precursor.* Electrochimica Acta, 1997. **42**(16): p. 2455-2464.

56. Balasubramanian, M., C.A. Melendres, and A.N. Mansour, *An X-ray absorption study of the local structure of cerium in electrochemically deposited thin films.* Thin Solid Films, 1999. **347**(1-2): p. 178-183.

57. Zhou, Y.C., R.J. Phillips, and J.A. Switzer, *Electrochemical Synthesis and Sintering of Nanocrystalline Cerium(Lv) Oxide Powders.* Journal of the American Ceramic Society, 1995. **78**(4): p. 981-985.

58. Inguanta, R., S. Piazza, and C. Sunseri, *Template electrosynthesis of CeO2 nanotubes.* Nanotechnology, 2007. **18**(48): p. -.

59. Bocchetta, P., M. Santamaria, and F. Di Quarto, *From ceria nanotubes to nanowires through electrogeneration of base.* Journal of Applied Electrochemistry, 2009. **39**(11): p. 2073-2081.

60. Zhitomirsky, I. and A. Petric, *Electrochemical deposition of yttrium oxide.* Journal of Materials Chemistry, 2000. **10**(5): p. 1215-1218.

61. Wang, A.Q. and T.D. Golden, *Anodic electrodeposition of cerium oxide thin films - I. Formation of crystalline thin films.* Journal of the Electrochemical Society, 2003. **150**(9): p. C616-C620.

62. Golden, T.D. and A.Q. Wang, *Anodic electrodeposition of cerium oxide thin films - II. Mechanism studies.* Journal of the Electrochemical Society, 2003. **150**(9): p. C621-C624.

63. Mahajan, S., et al., *Tuning plasmons on nano-structured substrates for NIR-SERS.* Physical Chemistry Chemical Physics, 2007. **9**(1): p. 104-109.

64. Shiu, J.Y., et al., *Fabrication of tunable superhydrophobic surfaces by nanosphere lithography.* Chemistry of Materials, 2004. **16**(4): p. 561-564.

65. Boneberg, J., et al., *The formation of nano-dot and nano-ring structures in colloidal monolayer lithography.* Langmuir, 1997. **13**(26): p. 7080-7084.

66. Burmeister, F., et al., *Colloid monolayers as versatile lithographic masks.* Langmuir, 1997. **13**(11): p. 2983-2987.

67. Spada, E.R., et al., *Homogeneous growth of antidot structures electrodeposited on Si by nanosphere lithography.* Journal of Applied Physics, 2008. **103**(11): p. -.

68. Haginoya, C., M. Ishibashi, and K. Koike, *Nanostructure array fabrication with a size-controllable natural lithography.* Applied Physics Letters, 1997. **71**(20): p. 2934-2936.

69. Dimitrov, A.S. and K. Nagayama, *Steady-State Unidirectional Convective Assembling of Fine Particles into 2-Dimensional Arrays.* Chemical Physics Letters, 1995. **243**(5-6): p. 462-468.

70. Onoda, G.Y. and E.G. Liniger, *Experimental-Determination of the Random-Parking Limit in 2 Dimensions.* Physical Review A, 1986. **33**(1): p. 715-716.

71. Mihi, A., M. Ocana, and H. Miguez, *Oriented colloidal-crystal thin films by spin-coating microspheres dispersed in volatile media.* Advanced Materials, 2006. **18**(17): p. 2244-+.

72. Dimitrov, A.S. and K. Nagayama, *Continuous convective assembling of fine particles into two-dimensional arrays on solid surfaces.* Langmuir, 1996. **12**(5): p. 1303-1311.

73. Trau, M., D.A. Saville, and I.A. Aksay, *Field-induced layering of colloidal crystals.* Science, 1996. **272**(5262): p. 706-709.

74. Hayward, R.C., D.A. Saville, and I.A. Aksay, *Electrophoretic assembly of colloidal crystals with optically tunable micropatterns.* Nature, 2000. **404**(6773): p. 56-59.

75. Park, S.H., D. Qin, and Y. Xia, *Crystallization of mesoscale particles over large areas.* Advanced Materials, 1998. **10**(13): p. 1028-+.

76. Scientific, T. *NIST Traceable Particle Size Standards*.

77. Hamlaoui, Y., et al., *Cathodic electrodeposition of cerium based oxides on carbon steel from concentrated cerium nitrate. Part II: Influence of electrodeposition parameters and of the addition of PEG.* Materials Chemistry and Physics, 2010. **120**(1): p. 172-180.

78. Arurault, L., B. Daffos, and F.X. Sauvage, *Nanocrystallized ceria-based coatings prepared by electrochemistry on TA6V titanium alloy.* Materials Research Bulletin, 2008. **43**(4): p. 796-805.

79. Zhou, Y.C. and J.A. Switzer, *Growth of cerium(IV) oxide films by the electrochemical generation of base method.* Journal of Alloys and Compounds, 1996. **237**(1-2): p. 1-5.

80. Arurault, L., et al., *Electrochemical preparation of adherent ceria coatings on ferritic stainless steel.* Thin Solid Films, 2004. **466**(1-2): p. 75-80.

81. Bocchetta, P., M. Santamaria, and F. Di Quarto, *Cerium oxyhydroxide nanowire growth via electrogeneration of base in nonaqueous electrolytes.* Electrochemical and Solid State Letters, 2008. **11**(9): p. K93-K97.

82. Aldykiewicz, A.J., A.J. Davenport, and H.S. Isaacs, *Studies of the formation of cerium-rich protective films using x-ray absorption near-edge spectroscopy and rotating disk electrode methods.* Journal of the Electrochemical Society, 1996. **143**(1): p. 147-154.

83. Li, G.R., et al., *Microstructural evolution of CeO2 from porous structures to clusters of nanosheet arrays assisted by gas bubbles via electrodeposition.* Langmuir, 2008. **24**(8): p. 4254-4259.

84. Hayes, S.A., et al., *The phase stability of cerium species in aqueous systems - I. E-pH diagram for the Ce-HClO4-H2O system.* Journal of the Electrochemical Society, 2002. **149**(12): p. C623-C630.

85. Yu, P., et al., *The phase stability of cerium species in aqueous systems - II. The Ce(III/IV)-H2O-H2O2/O-2 systems. Equilibrium considerations and pourbaix diagram calculations.* Journal of the Electrochemical Society, 2006. **153**(1): p. C74-C79.

86. Nobial, M., et al., *The nitrate reduction process: A way for increasing interfacial pH.* Journal of Electroanalytical Chemistry, 2007. **600**(1): p. 87-94.

87. Giannuzzi, L.A. and F.A. Stevie, *A review of focused ion beam milling techniques for TEM specimen preparation.* Micron, 1999. **30**(3): p. 197-204.

88. Jennings, A.T., M.J. Burek, and J.R. Greer, *Microstructure versus Size: Mechanical Properties of Electroplated Single Crystalline Cu Nanopillars.* Physical Review Letters, 2010. **104**(13): p. -.

89. Saitzek, S., et al., *Nanostructured ceria: a comparative study from X-ray diffraction, Raman spectroscopy and BET specific surface measurements.* Physica Status Solidi a-Applications and Materials Science, 2008. **205**(7): p. 1534-1539.

90. Weber, W.H., K.C. Hass, and J.R. Mcbride, *Raman-Study of Ceo2 - 2nd-Order Scattering, Lattice-Dynamics, and Particle-Size Effects.* Physical Review B, 1993. **48**(1): p. 178-185.

91. Kosacki, I., et al., *Raman scattering and lattice defects in nanocrystalline CeO2 thin films.* Solid State Ionics, 2002. **149**(1-2): p. 99-105.

92. Balasubramanian, M., C.A. Melendres, and A.N. Mansour, *X-ray absorption spectroscopy study of the local structure of heavy metal ions incorporated into electrodeposited nickel oxide films.* Journal of the Electrochemical Society, 1999. **146**(2): p. 607-614.

93. Phok, S. and R.N. Bhattacharya, *Effect of samarium doping on electrodeposited CeO2 thin film.* Physica Status Solidi a-Applications and Materials Science, 2006. **203**(15): p. 3734-3742.

94. Lai, W. and S.M. Haile, *Impedance spectroscopy as a tool for chemical and electrochemical analysis of mixed conductors: A case study of ceria.* Journal of the American Ceramic Society, 2005. **88**(11): p. 2979-2997.

95. Chang, H.Y. and H.I. Chen, *Morphological evolution for CeO2 nanoparticles synthesized by precipitation technique.* Journal of Crystal Growth, 2005. **283**(3-4): p. 457-468.

96. Sepa, D.B., M.V. Vojnovic, and A. Damjanovic, *Reaction Intermediates as a Controlling Factor in the Kinetics and Mechanism of Oxygen Reduction at Platinum-Electrodes.* Electrochimica Acta, 1981. **26**(6): p. 781-793.

97. M. E. Orazem, B.T., *Electrochemical Impedance Spectroscopy*. 2008: John Wiley & Sons.

98. Edwards, J.D. and F. Keller, *Formation of Anodic Coatings on Aluminum.* Transactions of The Electrochemical Society, 1941. **79**(1): p. 135-144.

99. Hunter, M.S. and P. Fowle, *Factors Affecting the Formation of Anodic Oxide Coatings.* Journal of the Electrochemical Society, 1954. **101**(10): p. 514-519.

100. Houser, J.E. and K.R. Hebert, *The role of viscous flow of oxide in the growth of self-ordered porous anodic alumina films.* Nature Materials, 2009. **8**(5): p. 415-420.

101. Skeldon, P., et al., *A tracer study of porous anodic alumina.* Electrochemical and Solid State Letters, 2006. **9**(11): p. B47-B51.

102. Garcia-Vergara, S.J., et al., *Compositional evidence for flow in anodic films on aluminum under high electric fields.* Journal of the Electrochemical Society, 2007. **154**(9): p. C540-C545.

103. Matefi-Tempfli, S. and M. Matefi-Tempfli, *Vertically Aligned Nanowires on Flexible Silicone using a Supported Alumina Template prepared by Pulsed Anodization.* Advanced Materials, 2009. **21**(40): p. 4005-+.

104. Fan, Z.Y., et al., *Electrical and photoconductive properties of vertical ZnO nanowires in high density arrays.* Applied Physics Letters, 2006. **89**(21): p. -.

105. Yasui, N., A. Imada, and T. Den, *Electrodeposition of (001) oriented CoPt L1(0) columns into anodic alumina films.* Applied Physics Letters, 2003. **83**(16): p. 3347-3349.

106. Fusil, S., et al., *Nanolithography based contacting method for electrical measurements on single template synthesized nanowires.* Nanotechnology, 2005. **16**(12): p. 2936-2940.

107. Sander, M.S., et al., *Template-assisted fabrication of dense, aligned arrays of titania nanotubes with well-controlled dimensions on substrates.* Advanced Materials, 2004. **16**(22): p. 2052-+.

108. Yang, Y., et al., *Anodic alumina template on Au/Si substrate and preparation of CdS nanowires.* Solid State Communications, 2002. **123**(6-7): p. 279-282.

109. Vlad, A., et al., *Nanowire-decorated microscale metallic electrodes.* Small, 2008. **4**(5): p. 557-560.

110. Chong, M.A.S., et al., *Combinational template-assisted fabrication of hierarchically ordered nanowire arrays on substrates for device applications.* Applied Physics Letters, 2006. **89**(23): p. -.

111. Colvin, V.L., *From opals to optics: Colloidal photonic crystals.* Mrs Bulletin, 2001. **26**(8): p. 637-641.

112. Yu, X.D., et al., *Filling fraction dependent properties of inverse opal metallic photonic crystals.* Advanced Materials, 2007. **19**(13): p. 1689-+.

113. Chung, Y.W., et al., *Fabrication of various nickel nanostructures by manipulating the one-step electrodeposition process.* Journal of the Electrochemical Society, 2007. **154**(6): p. E77-E83.

114. Bartlett, P.N., T. Dunford, and M.A. Ghanem, *Templated electrochemical deposition of nanostructured macroporous PbO2.* Journal of Materials Chemistry, 2002. **12**(10): p. 3130-3135.

115. Bartlett, P.N., et al., *Optical properties of nanostructured metal films.* Faraday Discussions, 2004. **125**: p. 117-132.

116. Yan, H.W., et al., *Fabrication of 2D and 3D ordered porous ZnO films using 3D opal templates by electrodeposition.* Electrochemistry Communications, 2005. **7**(11): p. 1117-1121.

117. Zhu, R., et al., *Controlling the electrodeposition of mesoporous metals for nanoplasmonics.* Nanoscale, 2009. **1**(3): p. 355-359.

118. Holland, B.T., et al., *Synthesis of highly ordered, three-dimensional, macroporous structures of amorphous or crystalline inorganic oxides, phosphates, and hybrid composites.* Chemistry of Materials, 1999. **11**(3): p. 795-805.

119. Wang, T.W., et al., *Preparation of a large Mesoporous CeO2 with crystalline walls using PMMA colloidal crystal templates.* Colloid and Polymer Science, 2006. **285**(1): p. 1-9.

120. Waterhouse, G.I.N., et al., *Physical and optical properties of inverse opal CeO2 photonic crystals.* Chemistry of Materials, 2008. **20**(3): p. 1183-1190.

121. Zhao, J.P., et al., *Fabrication of three-dimensionally ordered macroporous gadolinia-doped ceria films.* New Journal of Chemistry, 2008. **32**(6): p. 1014-1019.

122. Zhou, W., et al., *A novel efficient oxide electrode for electrocatalytic oxygen reduction at 400-600 degrees C.* Chemical Communications, 2008(44): p. 5791-5793.

123. Kim, S., et al., *Anomalous Electrical Conductivity of Nanosheaves of CeO2.* Chemistry of Materials, 2009. **21**(7): p. 1182-1186.

124. Yu, K.L., et al., *Convenient synthesis of CeO2 nanotubesl.* Materials Science and Engineering B-Solid State Materials for Advanced Technology, 2007. **139**(2-3): p. 197-200.

125. Gulbransen, E.A., T.P. Copan, and K.F. Andrew, *Oxidation of Copper between 250-Degrees-C and 450-Degrees-C and the Growth of Cuo Whiskers.* Journal of the Electrochemical Society, 1961. **108**(2): p. 119-123.

126. Jiang, X.C., T. Herricks, and Y.N. Xia, *CuO nanowires can be synthesized by heating copper substrates in air.* Nano Letters, 2002. **2**(12): p. 1333-1338.

127. Kumar, A., et al., *The effect of growth parameters on the aspect ratio and number density of CuO nanorods.* Journal of Physics-Condensed Matter, 2004. **16**(47): p. 8531-8543.

128. Zhang, K.L., et al., *Synthesis of large-area and aligned copper oxide nanowires from copper thin film on silicon substrate.* Nanotechnology, 2007. **18**(27): p. -.

129. Chopra, N., B. Hu, and B.J. Hinds, *Selective growth and kinetic study of copper oxide nanowires from patterned thin-film multilayer structures.* Journal of Materials Research, 2007. **22**(10): p. 2691-2699.

130. Qin, Y., T. Staedler, and X. Jiang, *Preparation of aligned Cu nanowires by room-temperature reduction of CuO nanowires in electron cyclotron resonance hydrogen plasma.* Nanotechnology, 2007. **18**(3): p. -.